Final Technical Report *April 1975*

INDUCED-CURRENT INTERACTION WITH WAVES

By: K. A. GRAF D. E. TREMAIN H. GUTHART

Prepared for:

OFFICE OF NAVAL RESEARCH
FIELD PROJECTS PROGRAMS
CODE 418
ARLINGTON, VIRGINIA 22217

CONTRACT N00014-73-C-0444

Sponsored by

DEFENSE ADVANCED RESEARCH PROJECTS AGENCY
ARPA ORDER 2185

STANFORD RESEARCH INSTITUTE
Menlo Park, California 94025 · U.S.A.

STANFORD RESEARCH INSTITUTE
Menlo Park, California 94025 · U.S.A.

Final Technical Report

April 1975

INDUCED-CURRENT INTERACTION WITH WAVES

By: K. A. GRAF D. E. TREMAIN H. GUTHART

Prepared for:

OFFICE OF NAVAL RESEARCH
FIELD PROJECTS PROGRAMS
CODE 418
ARLINGTON, VIRGINIA 22217

CONTRACT N00014-73-C-0444
ARPA Order No. 2185
Program Code No. 5E20
Contract Date: 25 November 1972
Contract Expiration Date: 31 January 1975
Amount of Contract: $314,019
Principal Investigator: H. Guthart
(415) 326-6200, Ext. 2801

SRI Project 2621

This research was supported by the Advanced Research Projects Agency of the Department of Defense and was monitored by ONR under Contract No. N00014-73-C-0444.

Approved by:

T. MORITA, *Director*
Electromagnetic Sciences Laboratory

RAY L. LEADABRAND, *Executive Director*
Electronics and Radio Sciences Division

Copy No. 4

SECURITY CLASSIFICATION OF THIS PAGE (When Data Entered)

REPORT DOCUMENTATION PAGE

READ INSTRUCTIONS BEFORE COMPLETING FORM

1. REPORT NUMBER

2. GOVT ACCESSION NO

3. RECIPIENT'S CATALOG NUMBER

4. TITLE (and Subtitle)

INDUCED-CURRENT INTERACTION WITH WAVES,

5. TYPE OF REPORT & PERIOD COVERED

Final Technical Report, Covering the period 1 August 1974 to 31 January 1975,

6. PERFORMING ORG. REPORT NUMBER

SRI Project 2621

7. AUTHOR(s)

K. A. Graf, D. E. Tremain, H. Guthart

8. CONTRACT OR GRANT NUMBER(s)

N00014-73-C-0444

9. PERFORMING ORGANIZATION NAME AND ADDRESS

Stanford Research Institute
Menlo Park, California 94025

10. PROGRAM ELEMENT, PROJECT, TASK AREA & WORK UNIT NUMBERS

ARPA Order No. 2185
Program Code 5E20

11. CONTROLLING OFFICE NAME AND ADDRESS

Defense Advanced Research Projects Agency
1400 Wilson Boulevard
Arlington, Virginia 22209

12. REPORT DATE

April 1975

13. NO. OF PAGES

51

14. MONITORING AGENCY NAME & ADDRESS (if diff. from Controlling Office)

Office of Naval Research
800 North Quincy Street
Arlington, Virginia 22217

15. SECURITY CLASS. (of this report)

UNCLASSIFIED

15a. DECLASSIFICATION/DOWNGRADING SCHEDULE

N/A

16. DISTRIBUTION STATEMENT (of this report)

17. DISTRIBUTION STATEMENT (of the abstract entered in Block 20, if different from report)

18. SUPPLEMENTARY NOTES

19. KEY WORDS (Continue on reverse side if necessary and identify by block number)

Radar
Water waves
Surface currents

20. ABSTRACT (Continue on reverse side if necessary and identify by block number)

Microwave measurements have been made with a coherent radar in a wind-wave tank to determine the effect of induced current on backscatter. Perturbations were introduced into the wave structure by inducing a current in the water that flowed either with or against the wind. The effect of current on cross section was slight; the effect on the Doppler was much more pronounced. It was found that the wave components responsible for radar backscatter are predominantly free waves (that is, waves which travel at the dispersion velocity) rather than waves which are parasitic to (or locked to) the dominant waves.

DD FORM 1 JAN 73 1473

EDITION OF 1 NOV 65 IS OBSOLETE

SECURITY CLASSIFICATION OF THIS PAGE (When Date Entered)

332 500

CONTENTS

LIST OF ILLUSTRATIONS iv

LIST OF TABLES vi

I INTRODUCTION 1

II DESCRIPTION OF EXPERIMENT 3

III RESULTS AND DISCUSSION 6

A. Wind-Profile Measurements 6

B. Water-Flow Measurements 7

C. Radar Measurements 8

1. Bragg Scatter 8
2. Cross-Section Variations Along False Bottom . . . 9
3. Doppler Shift and Doppler Spread Along False Bottom 15
4. Cross-Section Variation with Wind Speed 16
5. Wind Speed Dependence of Doppler Shift and Spread 20

D. Wavestaff Results 20

IV PREDICTED PERTURBATION OF CROSS SECTION 31

V CONCLUSIONS 37

VI RECOMMENDATIONS 39

APPENDIX—WAVE DISPERSION 41

ACKNOWLEDGMENTS 44

REFERENCES 45

ILLUSTRATIONS

1	Side View of Wind-Wave Tank with False Bottom Installed	4
2	Variation in Wind Speed Above the Water Surface in the Wind-Wave Tank	6
3	Induced Current Over False Bottom, Measured 2 Inches Below Mean Surface with No Wind	7
4	X-Band Spectra for Different Induced-Current Conditions, and a Wind Speed of 5 m/s	11
5	K_a-Band Spectra for Different Induced-Current Conditions, and a Wind Speed of 5 m/s	12
6	Variation of X-Band Cross Sections with Distance due to 5-m/s Wind, Normalized by the Cross Section for No Flow	13
7	Variation of X-Band Cross Section with Distance due to 10-m/s Wind, Normalized by the Cross Section for No Flow	13
8	Variation of K_a-Band Cross Section with Distance due to 5-m/s Wind, Normalized by the Cross Section for No Flow	14
9	Variation of K_a-Band Cross Section with Distance due to 10-m/s Wind, Normalized by the Cross Section for No Flow	14
10	Wind-Speed Dependence of X-Band Cross Sections for $\theta = 45°$, Normalized by Cross Section for No Flow	18
11	Wind-Speed Dependence of K_a-Band Cross Sections for $\theta = 45°$, Normalized by Cross Section for No Flow	18
12	Wind-Speed Dependence of X-Band Cross Sections for $\theta = 70°$, Normalized by Cross Section for No Flow	19

13 Wind-Speed Dependence of K_a-Band Cross Sections for $\theta = 70^\circ$, Normalized by Cross Section for No Flow 19

14 Wind-Speed Dependence of X-Band Doppler Shift for $\theta = 45^\circ$ 21

15 Wind-Speed Dependence of X-Band Doppler Shift for $\theta = 70^\circ$ 21

16 Wind-Speed Dependence of K_a-Band Doppler Shift for $\theta = 45^\circ$ 22

17 Wind-Speed Dependence of K_a-Band Doppler Shift for $\theta = 70^\circ$ 22

18 Wavestaff PSDs Measured for Three Induced-Current Conditions 23

19 Peak Value of Power Spectral Density Functions at Positions Along the False Bottom 23

20 Phase Difference Between Two Spatially Separated Probes for a Wind Speed of 10 m/s 25

21 Wavenumber Spectra Inferred from Wavestaff Measurements for Three Induced-Current Conditions and Two Wind Speeds 28

22 Comparison of Measured and Calculated Doppler Shift Based on Surface Value of Currents 30

23 Calculated Spectral Perturbation vs Fetch for $k = 3.07\ cm^{-1}$ and $U_N = 5$ m/s 32

24 Calculated Spectral Perturbation vs Fetch for $k = 3.27\ cm^{-1}$ and $U_N = 10$ m/s 32

25 Calculated Spectral Perturbation vs Fetch for $k = 8.09\ cm^{-1}$ and $U_N = 5$ m/s 33

26 Calculated Spectral Perturbation vs Fetch for $k = 8.62\ cm^{-1}$ and $U_N = 10$ m/s 33

27 Comparison of Predicted Spectral Perturbations with Measured Cross-Section Perturbations 35

A-1 Velocity and Wavenumber Dependence on Frequency 42

TABLES

1	Summary of Scattering Parameters	9
2	Mean and Standard Deviation of Doppler Shift Along False Bottom	16
3	Mean and Standard Deviation of Half-Power Doppler Spread Along False Bottom	17
4	Doppler Spread for Various Conditions	24

I INTRODUCTION

At present, the interaction of ocean surface waves in the capillary and short gravity range with internal waves, and in particular the manner and degree with which surface currents modulate surface waves and influence radar backscatter, are being investigated from a theoretical viewpoint.[1,2]* To date, most experimental investigations in the area of internal-wave/surface-wave interactions have been concerned with long gravity waves. This report summarizes the results of an experimental inquiry that investigated how induced currents affected microwave backscatter.

Details of the experimental setup will be discussed in Section II. In the experiment, interval waves of the type that might be expected to propagate along thermoclines in the ocean were simulated in a wind-wave tank by water flow over a sinusoidally corrugated "false bottom." The false bottom induced periodic variations in water velocity with position in the tank, when a constant flow rate was produced by a mechanical pump; typical mean flow rates were on the order of 20 cm/s in either direction. Various constant wind speeds between 3.6 m/s and 12 m/s were used to produce a variety of "sea states" in the tank. The water surface was illuminated by horizontally polarized X-band and K_a-band radars. The backscattered signal was coherently detected, and analyzed to determine cross sections, the mean Doppler shift, and the Doppler spread. The variations of these quantities with wind speed, mean water flow velocity, and position over the false bottom were observed. In addition, data from

---

*References are listed at the end of the report.

resistance-wire wavestaffs were used to compute the temporal power-spectral-density (PSD) of wave-height fluctuations at various positions along the false bottom. These results will be presented in Section III, and discussed further in Section IV.

II DESCRIPTION OF EXPERIMENT

The SRI wind-wave tank is 9.1 m (30 ft) long and has a cross section of 1.83 m by 1.83 m (6 ft × 6 ft). The salinity of the water in the tank was adjusted to that of ocean water. In this experiment, surface currents were induced by pumping water over a shallow section 3.05 m (10 ft) long, and 1.83 m (6 ft) wide, as shown in Figure 1. The shallow section was corrugated with a wavelength of 1.22 m (4 ft), so that the mean induced current varied in a sinusoidal manner. The false bottom varied 5.08 cm (2 inches) peak-to-peak, so when the water depth was 17.8 cm (7 inches) at the shallowest position and 22.9 cm (9 inches) at the deepest, the induced current, which should vary inversely as water depth, varied about 25%. The actual current variation was measured with a hot-film anemometer for a variety of conditions. Care was taken to minimize the buildup of organic matter on the anemometer probe; organic matter can introduce serious errors in water flow measurements. It was found that a conical sensor, when used properly, gave excellent results. A pump, with a pumping capacity of about 3850 liters (1000 gallons) per minute, produced a mean current that was affected somewhat by wind speed, as described in the next section.

Two adjustable blowers, with a total capacity of 1.7×10^3 m^3/min, were used to blow wind over the surface of the water at mean velocities up to 12 m/s near the top of the tank. The maximum velocity that could be achieved using these blowers was about 18 m/s. Wind speed was measured with a hot-wire anemometer.

Coherent microwave radars, operating at 9.6 GHz (X-band) and 31 GHz (K_a-band) were installed in the wind-wave tank. These radars were

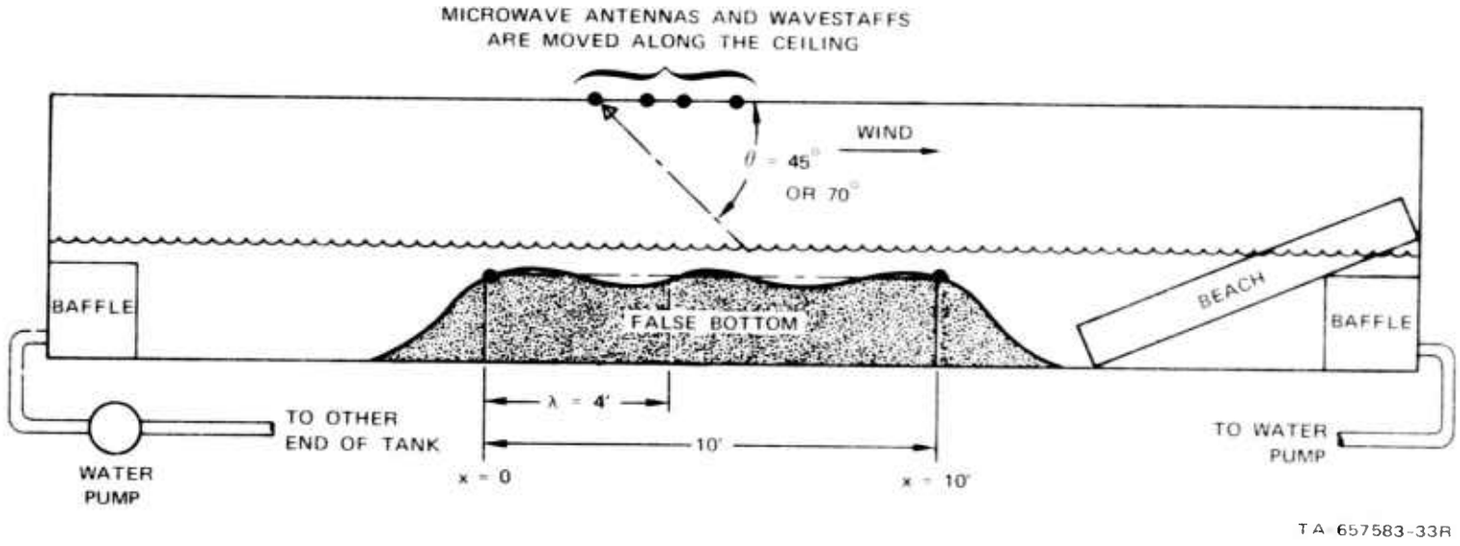

FIGURE 1 SIDE VIEW OF WIND-WAVE TANK WITH FALSE BOTTOM INSTALLED

operated in the backscatter mode. The polarization of the incident and received radiation was horizontal. The coherent radars allowed cross-sections and spectra to be measured at various positions along the corrugated false bottom. Data from the radars were analyzed in real time with the aid of a data acquisition system, consisting of an A-to-D converter controlled by a Hewlett-Packard 2100 computer system. A sampling rate of 400 Hz was used, and twenty 1024-point spectra were averaged for each experimental condition.

Direct wave-height measurements were made with resistance-wire wave staffs that were driven with ac signals from electronic bridge circuits. The wavestaff system and its use in measuring wave-height fluctuations have been described in detail previously.[3] Temporal PSDs of wave-height fluctuations were computed in real time, using the data acquisition system, at various positions along the false bottom. As in the case of the radar data, these PSDs consisted of averages of twenty 1024-point records. The wavestaff data were taken at positions on the water surface that were illuminated by the radars, in order to permit comparison of the radar data with wave-height data. In addition, cross-spectra between spatially separated wavestaffs were computed in order to establish the phase velocity of the waves under various wind and water-flow conditions.

III RESULTS AND DISCUSSION

A. Wind-Profile Measurements

The variation of wind velocity with distance above the water, for nominal wind velocities, U_N, of 5 and 10 m/s near the top of the tank, was measured with a hot-wire anemometer, and is shown in Figure 2 for points within 20 cm of the surface; the logarithmic variation of wind-speed near the surface specifies the frictional velocity, u_*, of the wind, and is the wind characteristic that should be used when comparing measurements in different facilities, or on the ocean surface.[4] For U_N values of 5 and 10 m/s, the frictional velocities were 19 cm/s and

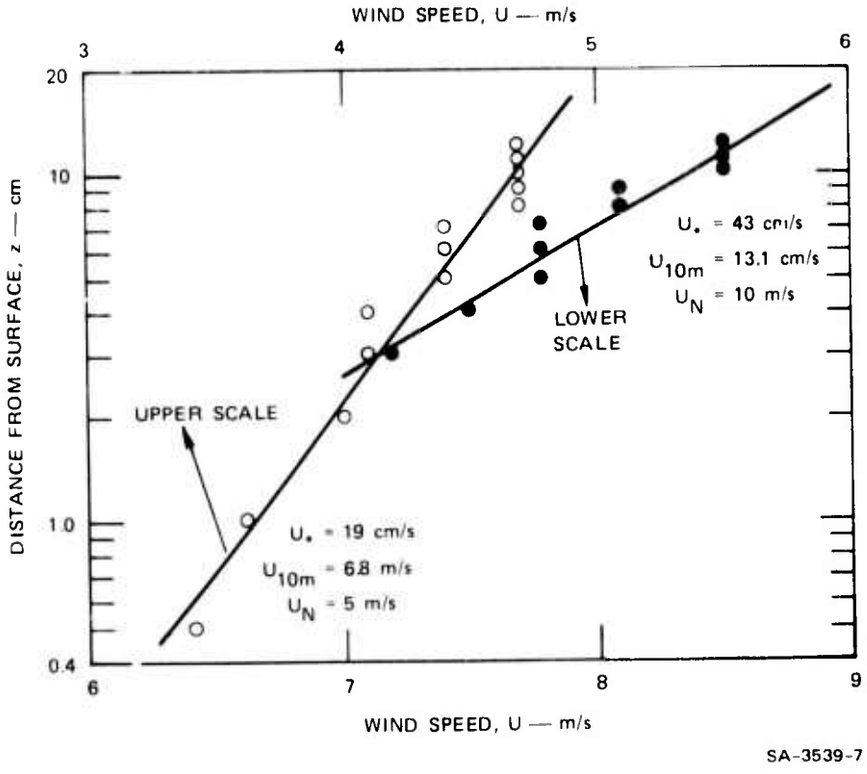

FIGURE 2 VARIATION IN WIND SPEED ABOVE THE WATER SURFACE IN THE WIND-WAVE TANK

43 cm/s, respectively. These values would correspond to wind velocities in the open ocean at a height of 10 m above the surface, U_{10m}, of 6.8 m/s (13.2 knots) and 13.1 m/s (22.5 knots), respectively.

B. Water-Flow Measurements

Flow measurements were made with a conical hot-film anemometer probe located 5.1 cm (2 inches) below the mean water surface. This was done in order to find the variation in drift velocity near the surface with position along the false bottom for the various flow conditions. It was not practicable to directly measure the velocity closer to the surface, because in the presence of the large-amplitude surface waves, the probe would not stay submerged all the time, and erroneous measurements would result.

The current distributions in the absence of wind, for pump-induced flow toward the beach, and flow away from the beach, are shown in Figure 3. The expected sinusoidal variation in flow velocity due to the sinusoidally corrugated false bottom is clearly seen in this figure;

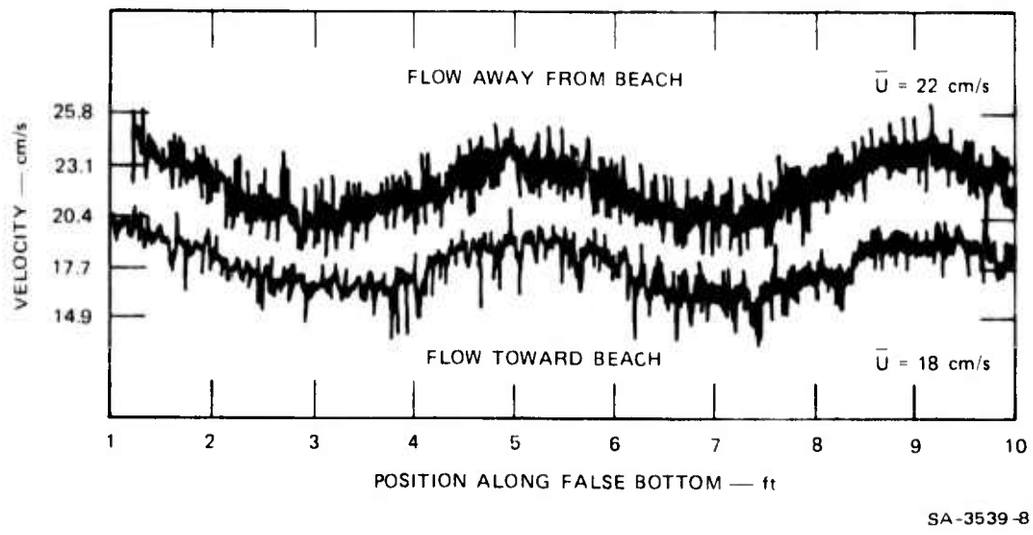

FIGURE 3 INDUCED CURRENT OVER FALSE BOTTOM, MEASURED 2 INCHES BELOW MEAN SURFACE WITH NO WIND

the maxima and minima in the velocity distributions correspond to the maxima and minima of the false bottom, respectively. The mean velocities were about 18 cm/s for flow toward the beach, and about -22 cm/s for flow away from the beach (the variation in mean flow velocity in the two directions is due to plumbing and pump characteristics). From vertical-profile data, it was inferred that the wind induced additional surface currents of 5 cm/s and 10 cm/s when U_N was 5 m/s and 10 m/s, respectively. The term "surface" current refers to conditions about half a centimeter below the actual surface. Closer to the surface, the wind will dominate the actual current.

C. Radar Measurements

1. Bragg Scatter

Bragg scatter theory predicts that, at an incident angle of θ, an electromagnetic wave of wavelength λ_m will backscatter from waves on the surface of wavelength λ_w, where λ_w is given by:

$$\lambda_w = \lambda_m/(2 \cos \theta)$$

$$k_w = k_m 2 \cos \theta$$

where the subscript m refers to microwave, and the subscript w refers to water waves. The corresponding wavelengths and wavenumbers k for the two frequencies and two angles of incidence for which measurements were made are summarized in Table 1.

If the water waves are traveling as "free" waves at the dispersion velocity, as shown in the Appendix, the corresponding velocity will be U(f), also listed in Table 1. The frequency at which such a wave would appear if there were no mean drift current is also listed.

Table 1

SUMMARY OF SCATTERING PARAMETERS

	X-Band (λ_m = 3.0 cm)		K_a-Band (λ_m = 1.0 cm)	
	θ = 45°	θ = 70°	θ = 45°	θ = 70°
λ_w, cm	2.12	4.38	0.707	1.46
k_w, cm^{-1}	2.96	1.43	8.89	4.29
U(f), cm/s	23.5	28.5	27	23
f, Hz, assuming no drift current	11.1	6.2	38	16

The Doppler frequency that can be expected is

$$f_D = \frac{2U_T \cos\theta}{\lambda_m} = U_T/\lambda_w \quad .$$

At first glance the last expression makes the Doppler shift appear independent of incident angle, but it is not, of course, since the wavelength responsible for scatter depends on θ. U_T is the total velocity with which the waves responsible for the scattering are moving. The data will be examined in a later section to determine if this velocity is the velocity of the dominant wave or the velocity specified by the dispersion relation for capillaries of the appropriate wavelength.

2. Cross-Section Variations Along False Bottom

Backscatter measurements were made at eight positions along the center of the wavetank for an incident angle of 45°. The antenna's

-3 dB width on the water surface along the length of the tank covered about one foot along the false bottom. Measurements were made for wind speeds of 5 m/s and 10 m/s and for three water-flow conditions. The flow conditions used were "no flow" (pump turned off), "flow with wind" (pumping toward the beach), and "flow against wind" (pumping away from the beach). Typical power spectral plots are shown in Figures 4 and 5 for one wind condition. Note that each of these plots is an average of twenty 1024-point records. The dynamic range in each case is at least 40 dB. Figures 4 and 5 were measured with the radar patch over the maximum in the false bottom that is the closest to the beach. The radar cross section (which is proportional to total received power) was calculated at eight positions along the false bottom. The cross sections were obtained by integrating under the power-versus-frequency curves, when plotted with a linear vertical and horizontal scale. This allowed a measurement that was less contaminated by noise spikes and spurious tank reflections, since such spurious contributions could be identified in the spectra and omitted from the integration. Typically, the probable error in a cross section measurement is estimated to be less than 2 dB. On the average, for these wind and flow conditions flow against wind tends to produce the largest cross section, while flow with wind tends to produce the smallest cross section.

In order to remove possible variations in the flow with wind and flow against wind measurements due to day-to-day systematic errors, the cross-section data were normalized to the no flow (i.e., pump turned off) results. The resulting data are plotted in Figures 6 through 9. The x coordinate in these figures is measured in feet relative to the leading edge of the false bottom. A tendency of the flow-against-wind cross section is clearly seen in Figures 6, 7, and 9. The two cross sections are quite similar in Figure 8, although both tend to increase with increasing fetch. For a 5 m/s wind at X-band, no variation is observed for flow against the wind and a 2 dB decrease near the leading

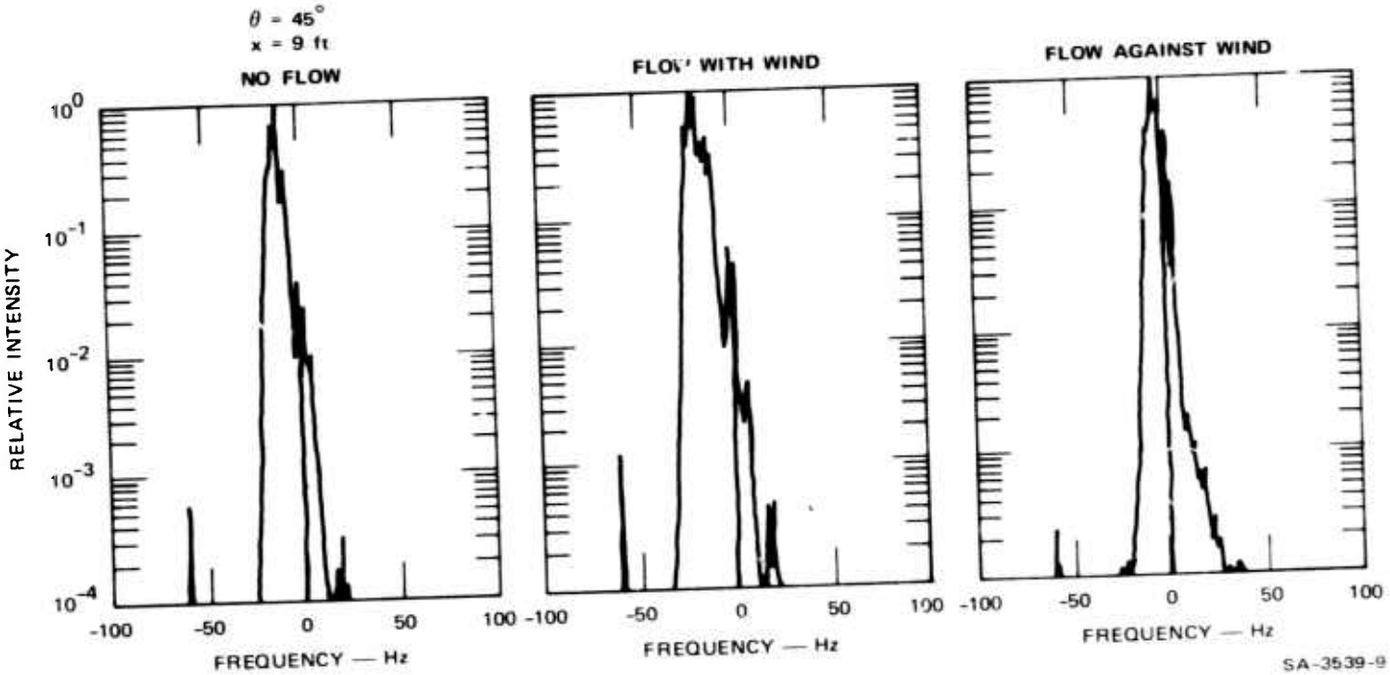

FIGURE 4 X-BAND SPECTRA FOR DIFFERENT INDUCED-CURRENT CONDITIONS, AND A WIND SPEED OF 5 m/s

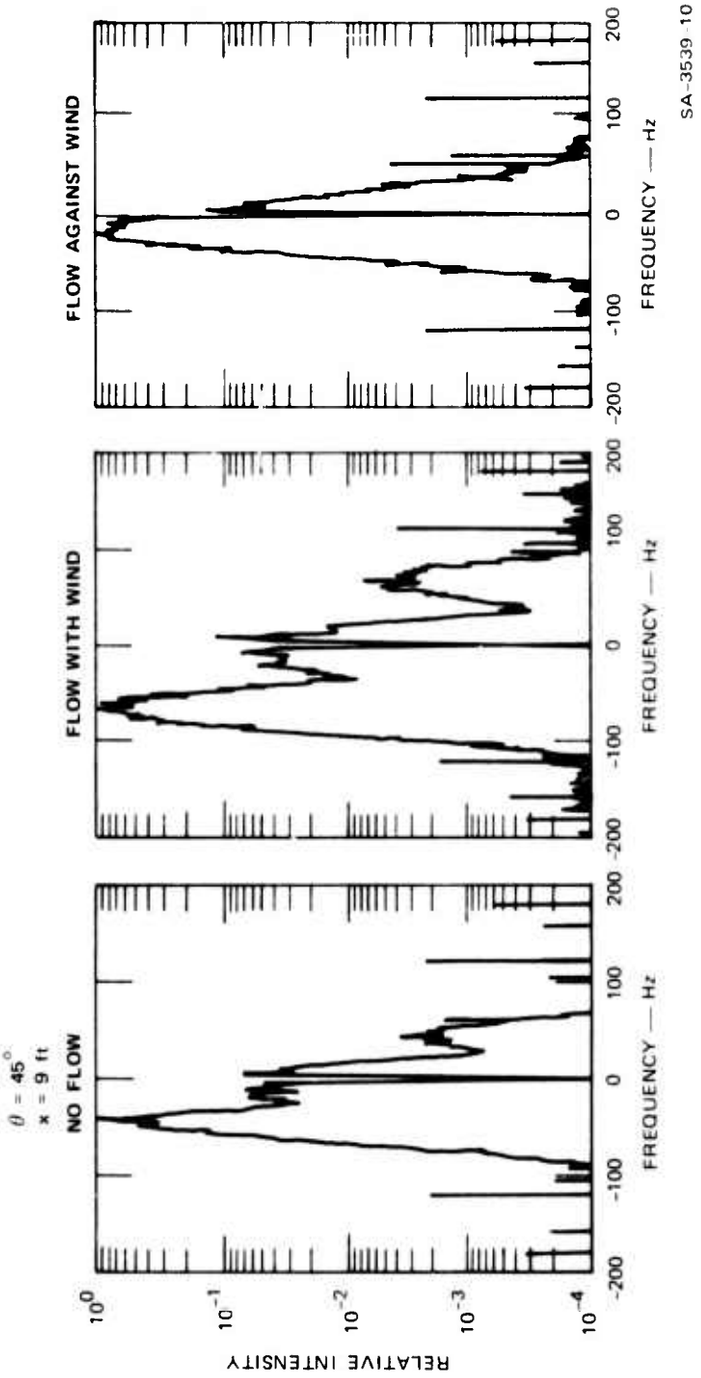

FIGURE 5 K_a-BAND SPECTRA FOR DIFFERENT INDUCED-CURRENT CONDITIONS, AND A WIND SPEED OF 5 m/s

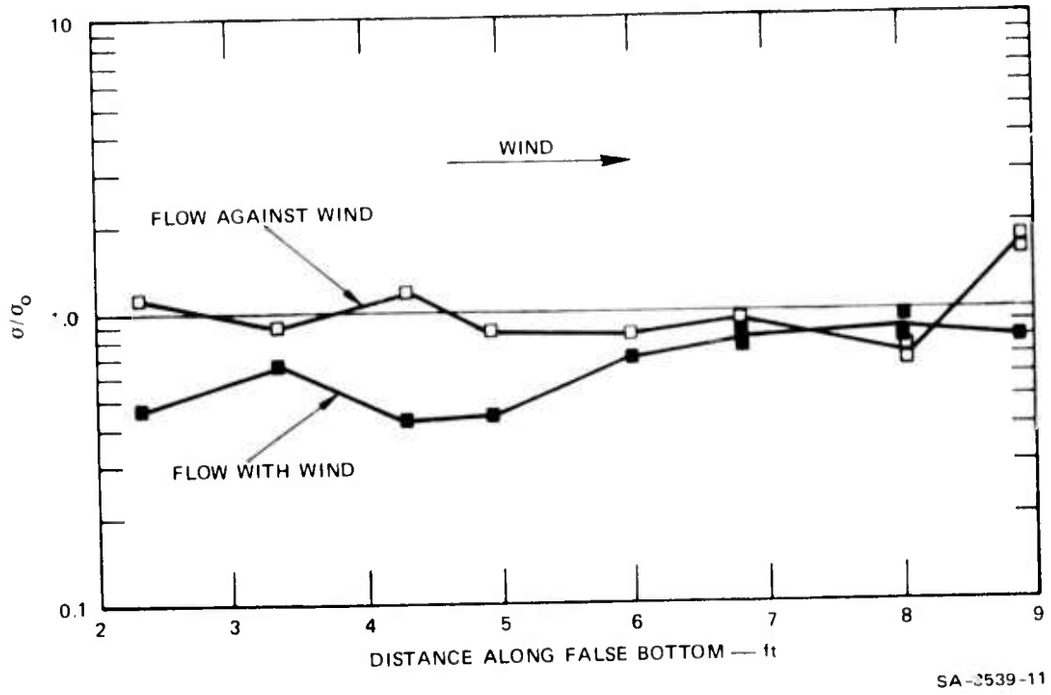

FIGURE 6 VARIATION OF X-BAND CROSS SECTIONS WITH DISTANCE DUE TO 5-m/s WIND, NORMALIZED BY THE CROSS SECTION FOR NO FLOW

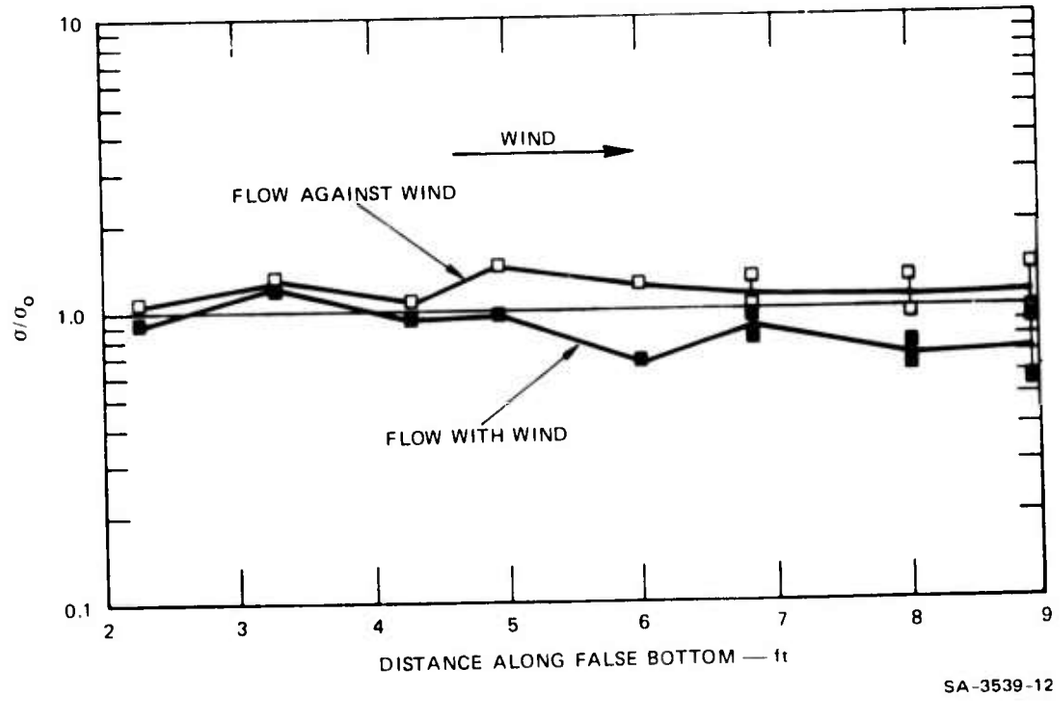

FIGURE 7 VARIATION OF X-BAND CROSS SECTION WITH DISTANCE DUE TO 10-m/s WIND, NORMALIZED BY THE CROSS SECTION FOR NO FLOW

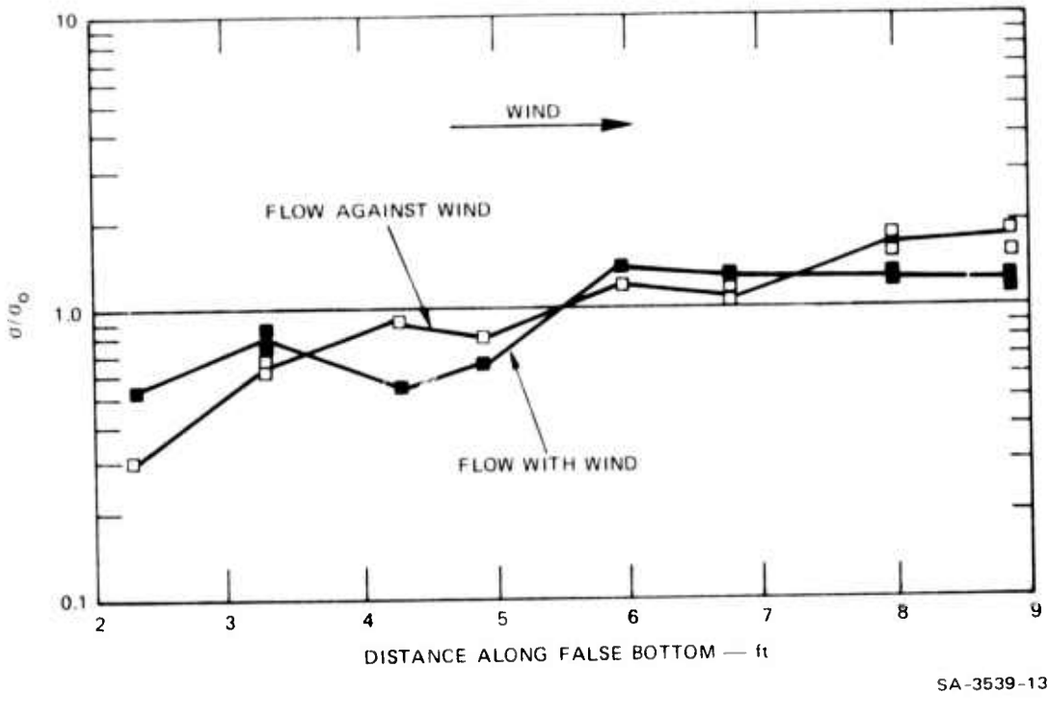

FIGURE 8 VARIATION OF K_a-BAND CROSS SECTION WITH DISTANCE DUE TO 5-m/s WIND, NORMALIZED BY THE CROSS SECTION FOR NO FLOW

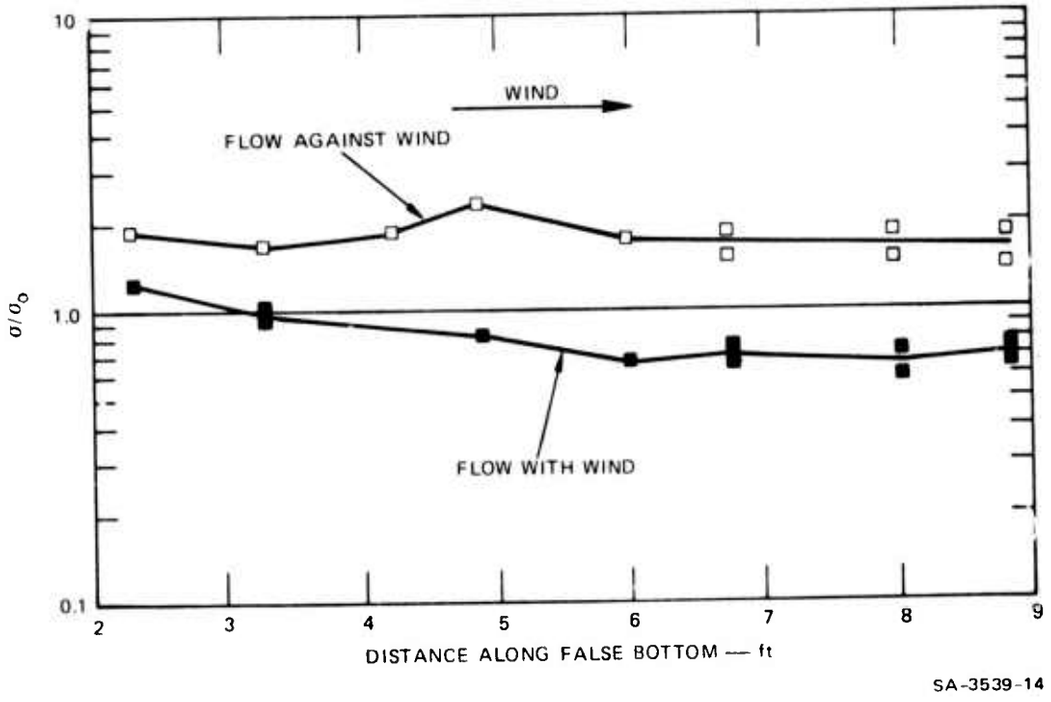

FIGUFE 9 VARIATION OF K_a-BAND CROSS SECTION WITH DISTANCE DUE TO 10-m/s WIND, NORMALIZED BY THE CROSS SECTION FOR NO FLOW

edge of the false bottom is seen for the opposite flow condition. At K_a-band with a 5 m/s wind, a 2-dB decrease near the leading edge is observed for flow with the wind and a 3-dB decrease near the leading edge is seen for the opposite flow condition. On the average, for 10 m/s wind at X-band, the cross-section data for flow against the wind is about 2-dB higher than for flow with the wind. The ratio of flow-against-wind cross section to flow-with-wind cross section in Figure 9 (K_a band, 10 m/s) is at most about 4 dB. This is the largest change that is seen in Figures 6 through 9 for the various flow conditions. Since the change in mean water velocity between the two flow conditions is about 40 cm/s, it is perhaps not surprising that any change in cross section due to the 5 cm/s change in flow caused by the corrugated false bottom is not visible in these figures.

3. Doppler Shift and Doppler Spread Along False Bottom

The Doppler shift data shows no readily identifiable systematic variation with position along the false bottom; the mean Doppler-shift data and the standard deviation of the data are summarized in Table 2. The quantities in this table as well as those in Table 3 have been taken over all the measurements along the false bottom--that is, the means and standard deviations are spatial averages taken along the false bottom. The principal effects are the comparatively small Doppler shift associated with the flow-against-wind cases, the larger shifts associated with the no-flow cases, and the largest shift in the flow-with-wind cases. This is, of course, due to the fact that the waves are being convected by the surface current. The surface waves move toward the beach in all cases.

Table 2

MEAN AND STANDARD DEVIATION OF DOPPLER SHIFT
ALONG FALSE BOTTOM
(Flow conditions are the same as for data
in Figures 6 through 9)

Condition	Doppler Shift (Mean ± Standard Deviation) (Hz)	
	X-Band	K_a-Band
5 m/s no flow	-10.7 ± 0.5	-43.8 = 2.6
5 m/s flow with wind	-15.3 ± 0.9	-65.8 = 4.2
5 m/s flow against wind	-4.1 ± 0.6	-16.6 = 2.2
10 m/s no flow	-12.5 ± 0.7	-51.3 = 1.8
10 m/s flow with wind	-17.4 ± 1.0	-67.9 = 2.8
10 m/s flow against wind	-6.5 ± 0.8	-29.4 = 5.3

The Doppler spread, which is defined here to be equal to the half-power width, in hertz, of the measured spectra also showed no significant variation with position along the false bottom. The means and standard deviations of the Doppler-spread data are tabulated in Table 3.

4. Cross-Section Variation with Wind Speed

In order to see the effects of various wind speeds on cross section, Doppler shift, and Doppler spread, the radars were aimed at a

Table 3

MEAN AND STANDARD DEVIATION OF HALF-POWER
DOPPLER SPREAD ALONG FALSE BOTTOM
(Flow conditions are the same as for data
in Figures 6 through 9)

Condition	Doppler Spread (Mean ± Standard Deviation) (Hz)	
	X-Band	K_a-Band
5 m/s no flow	4.5 ± 1.4	14.1 ± 3.5
5 m/s flow with wind	6.0 ± 1.2	21.3 ± 3.1
5 m/s flow against wind	5.1 ± 1.2	18.8 ± 2.7
10 m/s no flow	7.1 ± 1.7	33.5 ± 5.1
10 m/s flow with wind	8.1 ± 0.9	30.9 ± 5.7
10 m/s flow against wind	10.6 ± 1.3	38.5 ± 7.7

patch over the central maximum on the false bottom and the wind speed and incident angle were varied. This was done largely to check the accuracy of a theoretical prediction[2] that has been made for the variation of cross section under certain flow conditions. The cross sections that were obtained for various wind speeds are plotted in Figures 10 through 13. These curves have also been normalized to the no-flow cross sections. The water flow velocities due to the pump are the same as for the data presented earlier. The normalized curves change rapidly for a wind speed of less than about 5 m/s because of a

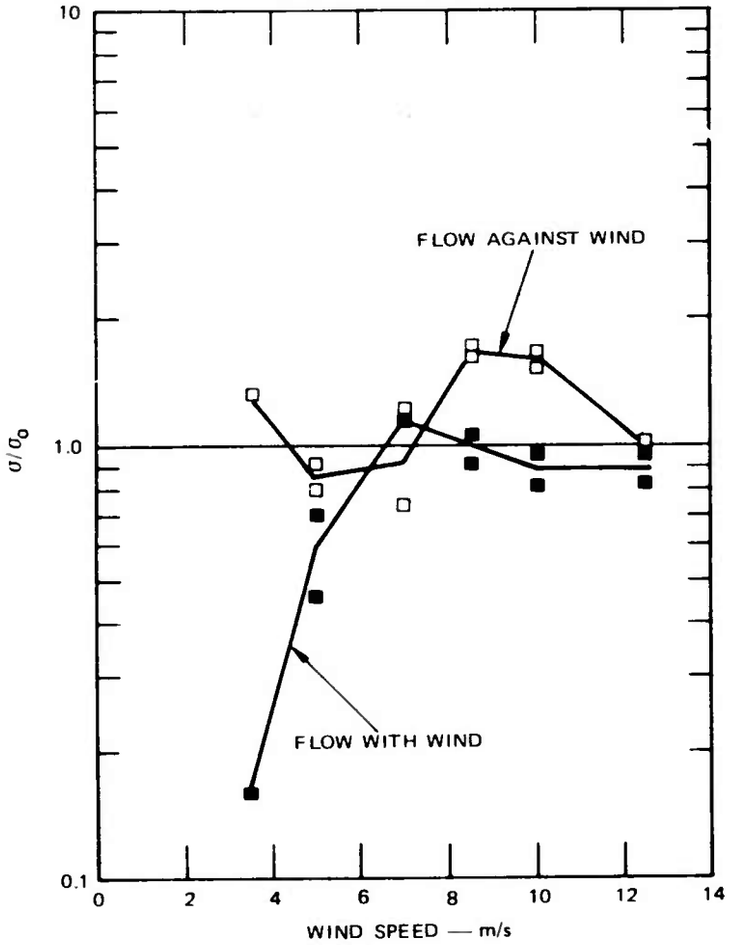

FIGURE 10 WIND-SPEED DEPENDENCE OF X-BAND CROSS SECTIONS FOR θ = 45°, NORMALIZED BY CROSS SECTION FOR NO FLOW

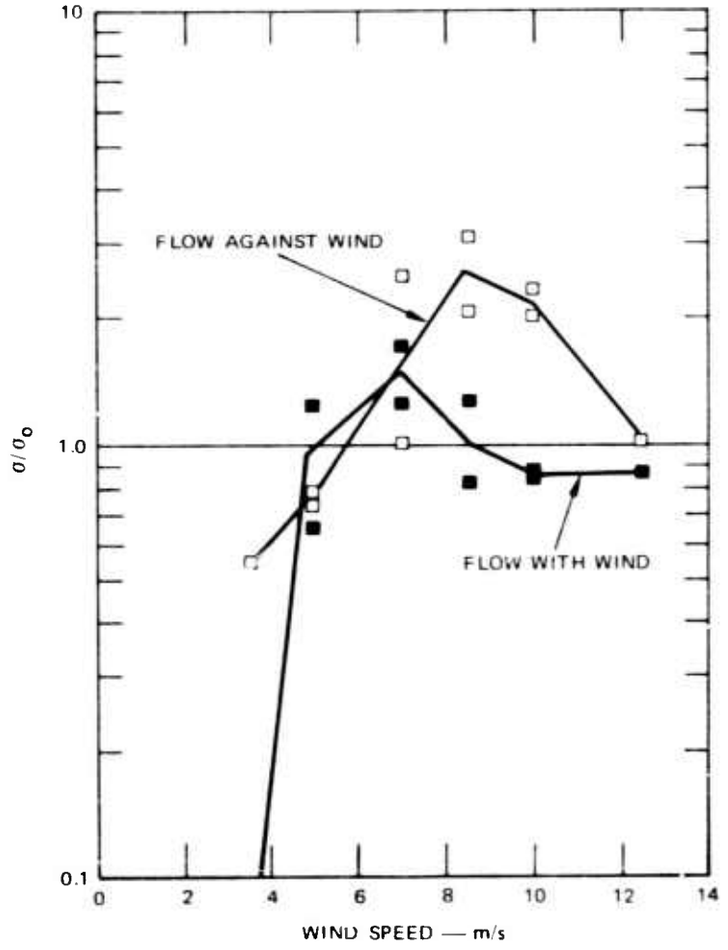

FIGURE 11 WIND-SPEED DEPENDENCE OF K_a-BAND CROSS SECTIONS FOR θ = 45°, NORMALIZED BY CROSS SECTION FOR NO FLOW

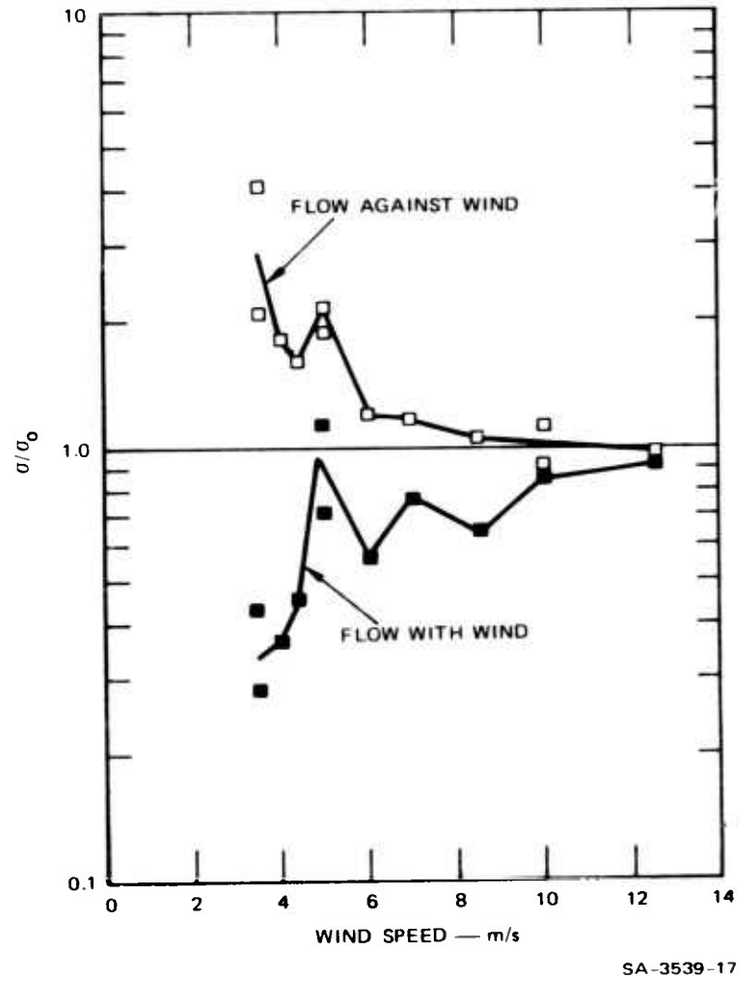

FIGURE 12 WIND-SPEED DEPENDENCE OF X-BAND CROSS SECTIONS FOR θ = 70°, NORMALIZED BY CROSS SECTION FOR NO FLOW

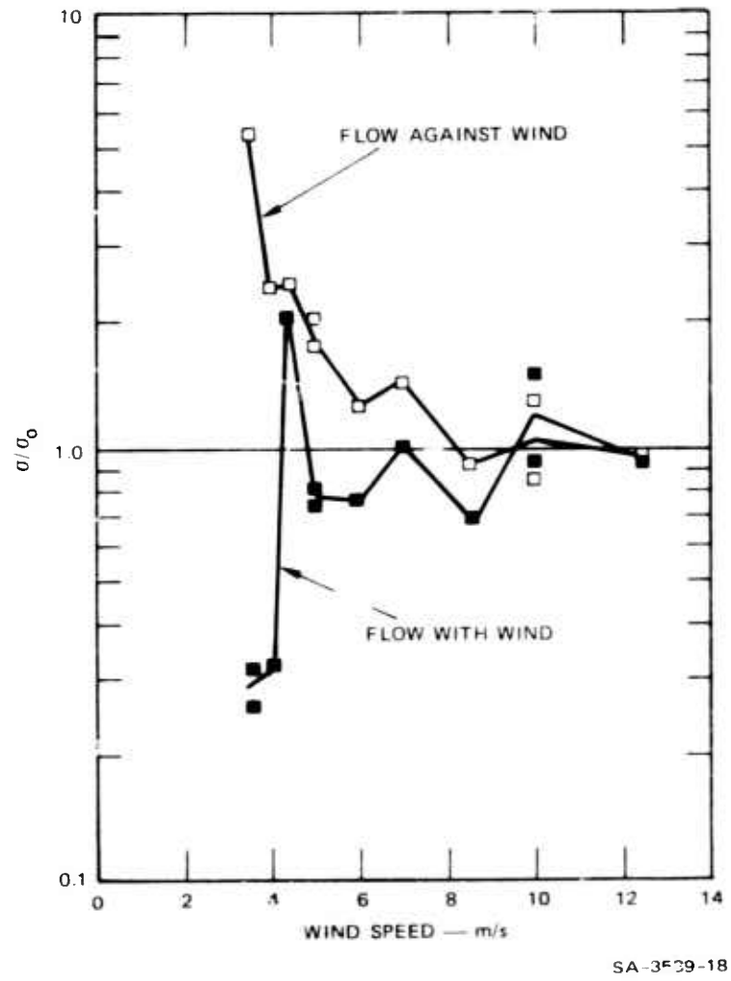

FIGURE 13 WIND-SPEED DEPENDENCE OF K_a-BAND CROSS SECTIONS FOR θ = 70°, NORMALIZED BY CROSS SECTION FOR NO FLOW

tendency for the induced current to perturb the waves in regions where they are developing. The induced current retards or speeds up the development of the wave spectra at any particular fetch and corresponding wind speed. These curves indicate that for incident angles of both 45° and 70° (as measured from the horizontal), the cross section tends to be greater when the water is being pumped against the wind than when it is being pumped with the wind, at least over the range of wind speeds indicated in the plots.

5. Wind Speed Dependence of Doppler Shift and Spread

The mean Doppler shifts for the conditions described in the preceding section are plotted in Figures 14 through 17. The principal effects seen in these plots are the expected tendencies of the flow-with-wind condition to produce the largest Doppler shifts, and of the flow-against-wind condition to produce the smallest Doppler shifts. The corresponding Doppler-spread data are summarized in Table 4. The Doppler spread tends to increase linearly with wind speed, which is intuitively reasonable because the surface becomes rougher with increasing wind speed and larger "dominant" waves develop. The Doppler spread can be related to the orbital velocity of the dominant wave.[5]

D. Wavestaff Results

Wavestaff data have been taken using a single resistance-wire probe at eight positions along the false bottom for wind speeds of 5 m/s and 10 m/s. The positions correspond to those on the water surface that had been illuminated by the radars. Typical results are shown in Figure 18 (these results were measured 6 feet from the leading edge of the false bottom; see Figure 19). It can be seen that the largest-amplitude dominant waves are produced when the water is pumped away from the beach, and the lowest-amplitude dominant waves are produced

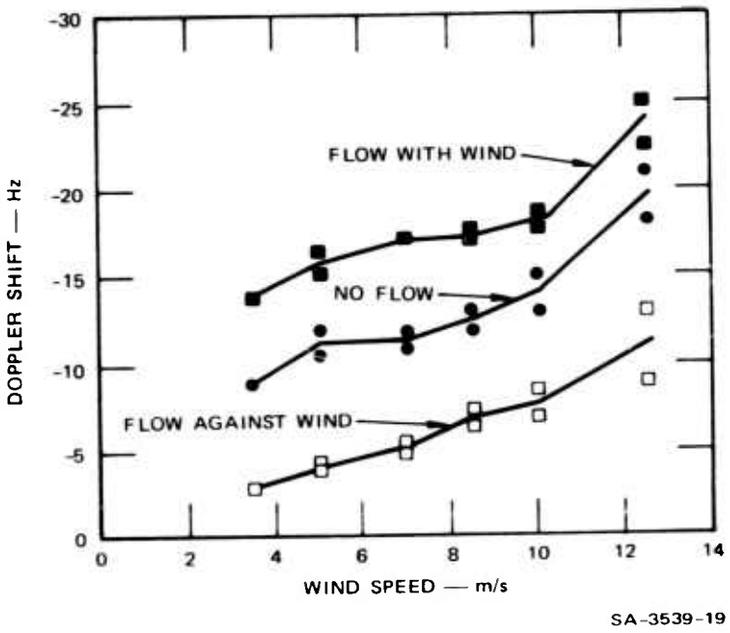

FIGURE 14 WIND-SPEED DEPENDENCE OF X-BAND DOPPLER SHIFT FOR θ = 45°

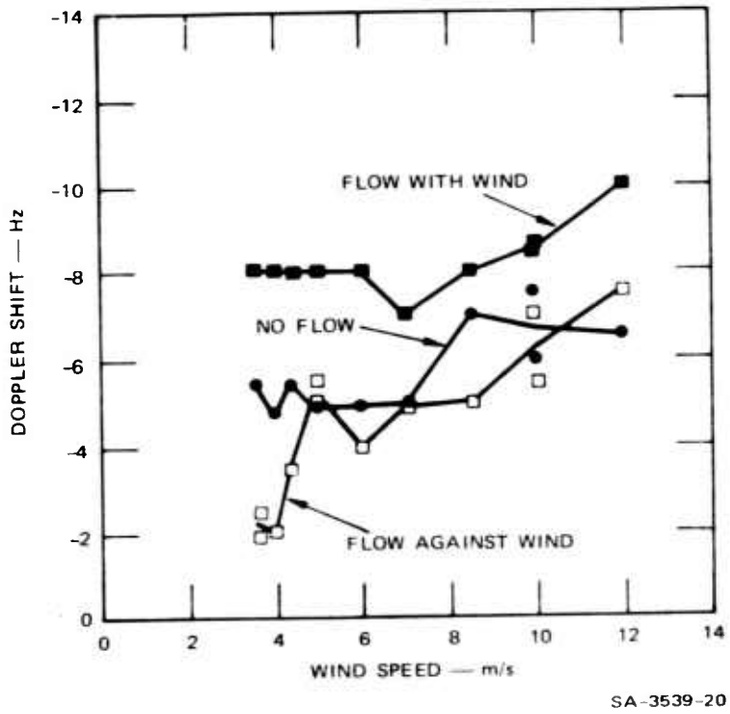

FIGURE 15 WIND-SPEED DEPENDENCE OF X-BAND DOPPLER SHIFT FOR θ = 70°

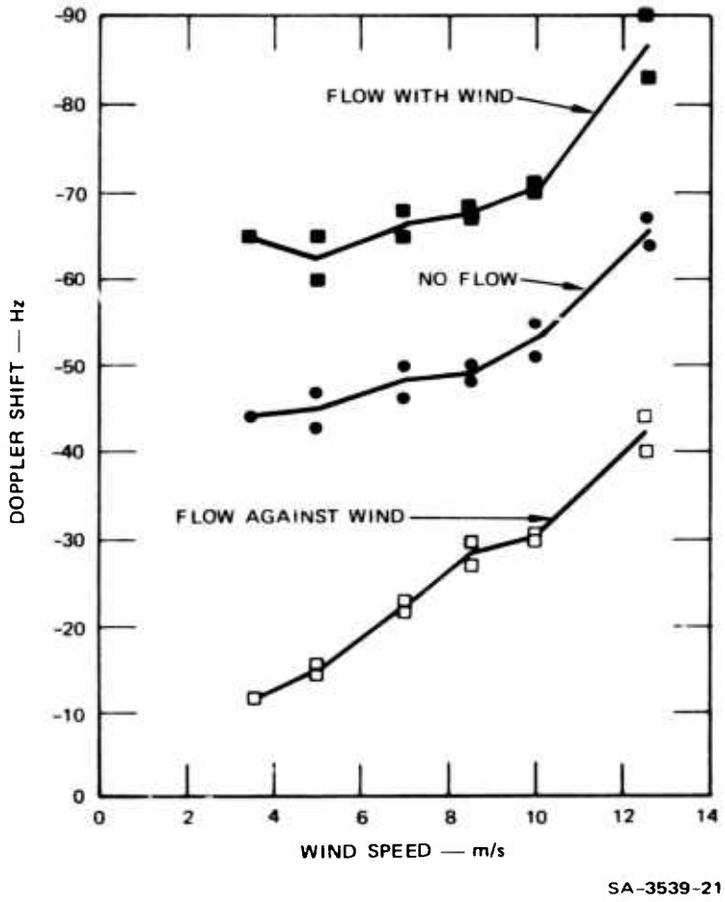

FIGURE 16 WIND-SPEED DEPENDENCE OF K_a-BAND DOPPLER SHIFT FOR θ 45°

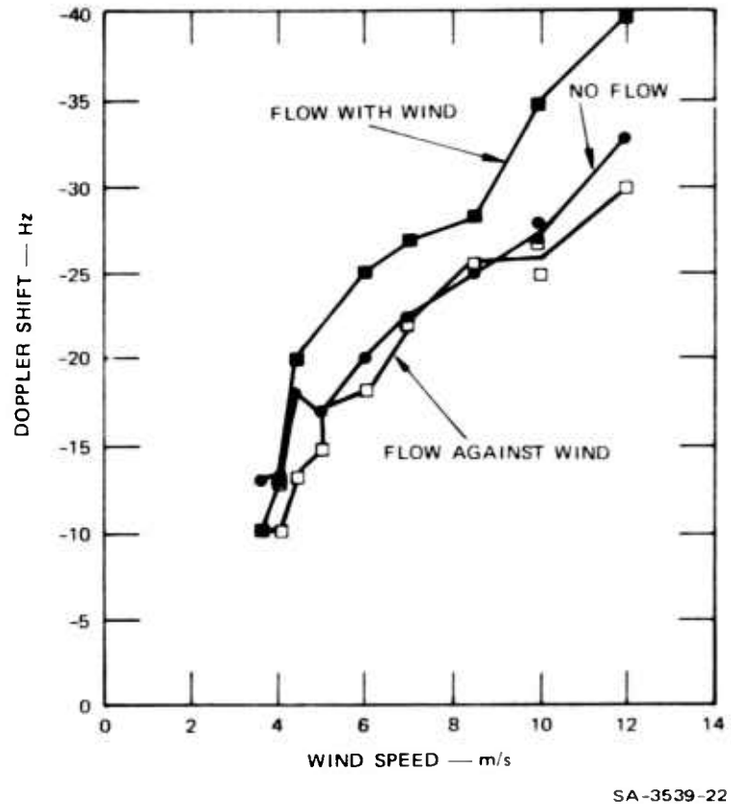

FIGURE 17 WIND-SPEED DEPENDENCE OF K_a-BAND DOPPLER SHIFT FOR θ = 70°

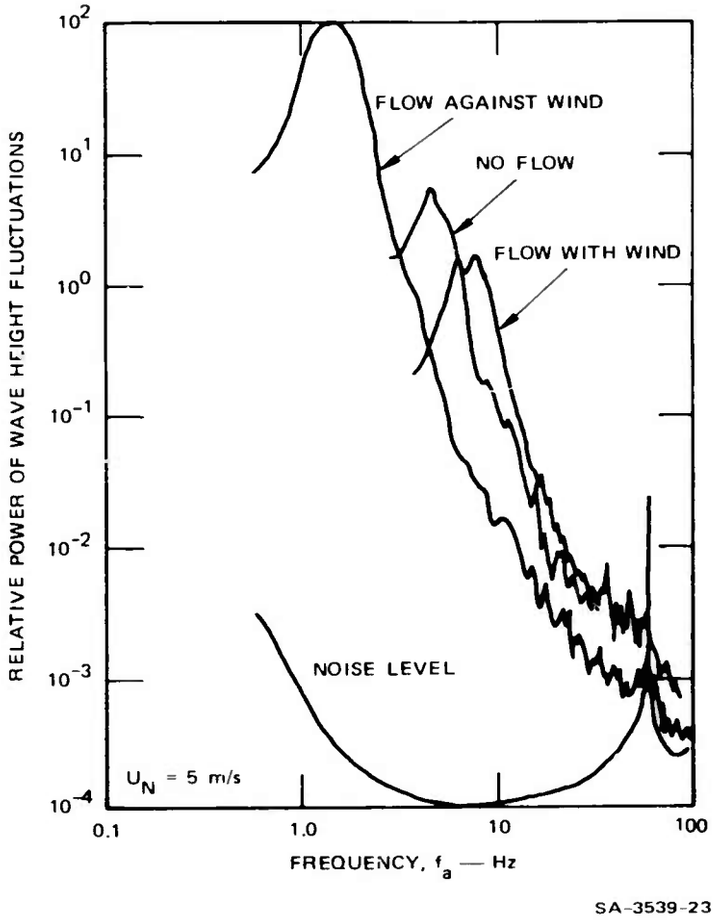

FIGURE 18 WAVESTAFF PSDs MEASURED FOR THREE INDUCED-CURRENT CONDITIONS

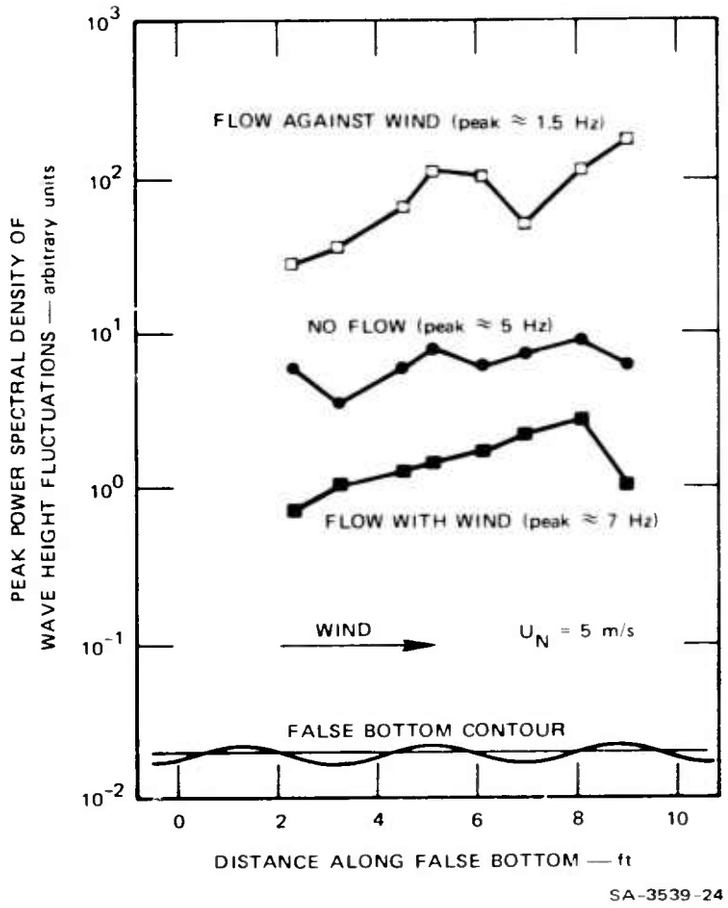

FIGURE 19 PEAK VALUE OF POWER SPECTRAL DENSITY FUNCTIONS AT POSITIONS ALONG THE FALSE BOTTOM

Table 4

DOPPLER SPREAD FOR VARIOUS CONDITIONS--LINEAR FIT TO DATA
[Doppler Spread (Hz) = A × Windspeed (m/s)
for wind speed less than 12 m/s]

Microwave Frequency and Incident Angle	Parameter A	
	Flow Against Wind	Flow with Wind, and No Flow
X-band $\theta = 45°$	1.1	0.7
X-band $\theta = 70°$	0.8	0.5
K_a-band $\theta = 45°$	4.0	2.9
K_a-band $\theta = 70°$	2.9	2.1

when the water is pumped toward the beach. The fetch dependence of the dominant wave is shown in Figure 19. The frequencies at which the wavestaff spectra peak are approximately independent of fetch; these frequencies are designated in Figure 19.

There does not appear to be as strong a fetch dependence for a 10-m/s wind speed. This may be because the waves build up more rapidly at the higher wind speed, and tend to be more nearly saturated than at the lower speed.

There is a tendency for a "bump" to be present in the wavestaff spectra at the second harmonic of the dominant frequency for the various flow conditions. This "second harmonic" effect has been observed and discussed in an earlier study.[3]

Figure 20 is a plot of the magnitude and phase of the cross spectrum (i.e., the Fourier transform of the cross-correlation function) for two wavestaff probes that were separated 0.94 cm along the length of the tank (i.e., parallel to the flow), and 0.34 cm along the width of the tank (i.e., perpendicular to the flow). This plot is for a wind speed of 10 m/s and for the no-flow condition, with the probes located slightly

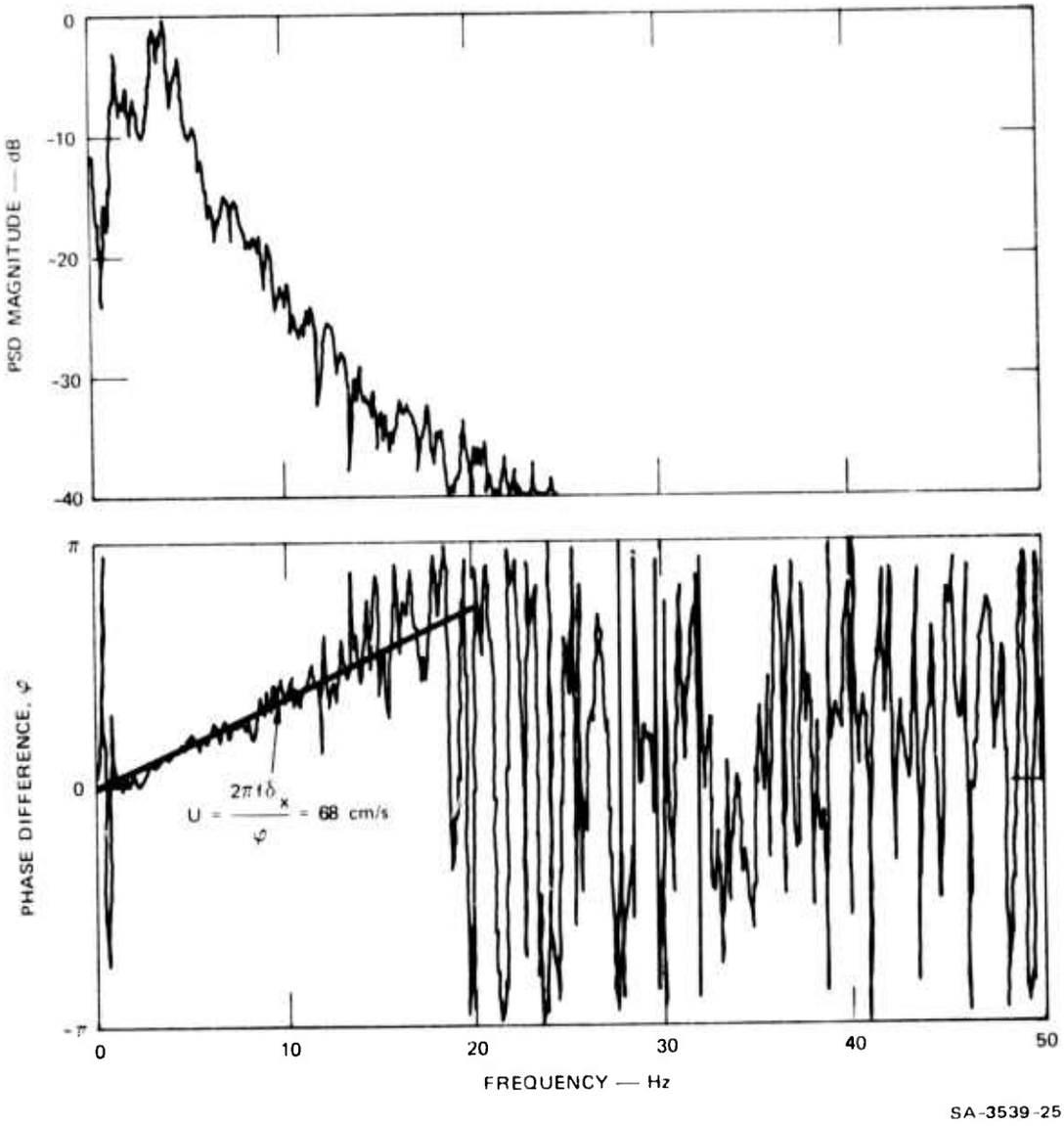

FIGURE 20 PHASE DIFFERENCE BETWEEN TWO SPATIALLY SEPARATED PROBES FOR A WIND SPEED OF 10 m/s

upwind of the false bottom. The phase is approximately a linear function of frequency out to at least 18 Hz. This implies that all wave components in this range travel at the same phase velocity. This phase velocity may be easily found, assuming that the flow between a given pair of wavestaffs that are separated a distance δ_x in the direction of flow is one-dimensional, by the relation

$$U = \frac{\omega \delta_x}{\varphi} \quad .$$

Here, U is the total velocity of the wave (drift velocity, if any, plus phase velocity), and ω is the angular frequency. Finding ω/φ from Figure 20 and substituting it into this formula gives U = 68 cm/s. The drift velocity at the surface due to a 10-m/s wind is approximately 10 cm/s, and the phase velocity of the waves in Figure 20 is about 58 cm/s. This is the velocity of a wave at a frequency of 2.6 Hz, according to the dispersion relation for gravity waves. It is concluded that all the wave components observed with the wavestaffs (at least below 18 Hz) are "locked" or "parasitic" to the fundamental or dominant wave. This effect has also been observed in an earlier study.[3] The observed total velocity of 68 cm/s is more than a factor of 2 higher than the velocities of the waves responsible for the bulk of the radar return at both X-band and K_a-band. It will be shown that the dominant wave and the components that are locked to it contribute very little to the radar return. Most of the radar return will be shown to be due to capillary waves, which travel at velocities independent of the longer gravity waves that dominate the wavestaff spectra.

On the basis of the previous analysis, the measured wavestaff data, of the type shown in Figure 18, were assumed to be transported at the velocity of the dominant wave plus the drift velocity. In this way, the frequency spectra were converted to wavenumber spectra. For example,

for a 5-m/s wind with flow against wind, the frequency spectrum peaks at 1.6 Hz. This apparent frequency f_a will differ from the frequency in the "moving water" due to the surface drift current U_D (U_D = -22 + 5 = -17 cm/s) by the relation

$$f = f_a \frac{U(f)}{[U(f) + U_D]} \quad .$$

By interaction, f can be found to be 2 Hz and U(f) 76 cm/s. Thus, the total velocity, including the effect of the drift current of -17 cm/s, is 59 cm/s. The total current can relate apparent frequency components to wavenumbers by the relation:

$$k_w = \frac{2\pi f}{U(f)}$$

$$= \frac{2\pi f_a}{[U(f) + U_o]} \quad .$$

Using this relation, the data in Figure 18 were plotted against wavenumber as shown in Figure 21. To a good approximation, $k_w = 0.11\ f_a$ for all the data at U_N = 5 m/s. For the data at U_N = 10 m/s, k_a = 0.086 f_a for no flow, 0.076 f_a for flow against wind, and 0.084 f_a for flow with wind. The 10-m/s data have also been plotted in Figure 21. It can be seen that there is very little difference in the wavenumber spectra due to changing wind except at low wavenumbers. The spectra continue to grow at low wavenumbers and appear "saturated" at higher wavenumbers. The induced current influences the spectra at all wavenumbers.

(The high-wavenumber ends of the spectra have not been plotted in Figure 21 because they are dominated by instrument noise that appears

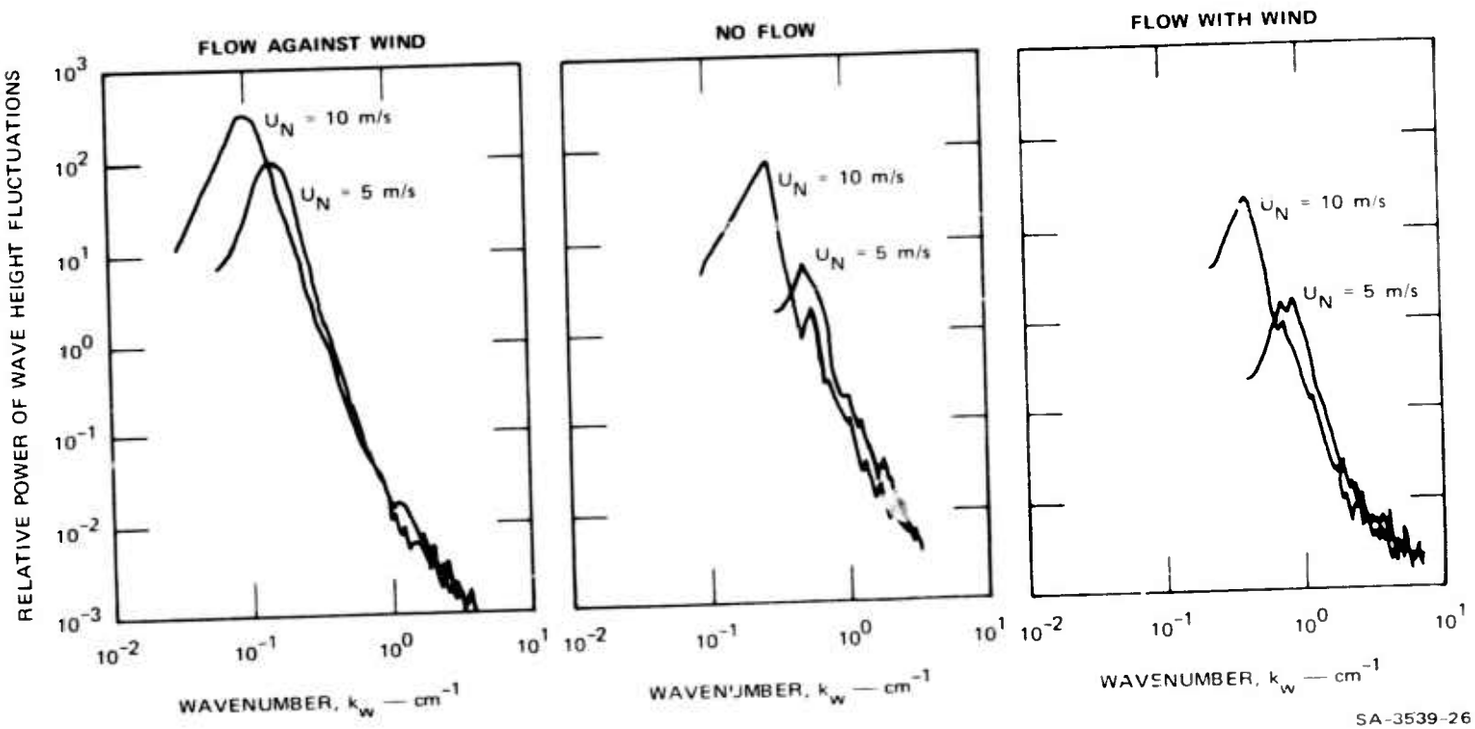

FIGURE 21 WAVENUMBER SPECTRA INFERRED FROM WAVESTAFF MEASUREMENTS FOR THREE INDUCED-CURRENT CONDITIONS AND TWO WIND SPEEDS

differently for each curve. For example, if all curves have a slightly different total velocity, the 60-Hz noise spike will show up at different wavenumbers for each condition.)

Since wavestaff data suggest that all the measured wave structure is moving at the velocity of the convected dominant wave, the microwave Doppler data were examined to see if the structure responsible for most of the backscatter was also traveling at that velocity, or at the velocity predicted by the dispersion relation. (The dispersion relation is shown in the Appendix.) It is important to know the relative extent to which microwaves scatter from parasitic and "free" waves. Figure 22 shows a comparison of the measured Doppler shift with the two corresponding calculated values. It is clear that microwaves scatter predominantly from the free waves.

The backscatter spectra were also examined to see if any signal could be detected at the Doppler frequency predicted for the parasitics. In all cases the signal could not be found, either because of the spread in the spectrum or because it was more than 30 dB below the peak. It was concluded that scattering by parasitic waves was negligible in this study.

The data shown in Figure 22 are in groups of three. In all cases, the lowest measured Doppler is due to flow against the wind and the highest is due to flow with the wind. Notice that the calculation based on the velocity of the dominant wave is approximately independent of current flow. This is because flow against the wind produces a larger (longer wavelength) wave that moves faster in still water but at almost the same total velocity in the water being pumped upwind. Similarly, flow with the wind produces a shorter-wavelength, slower dominant wave that reaches the same total velocity only because it is convected downwind by the (5 cm/s or 10 cm/s) induced current.

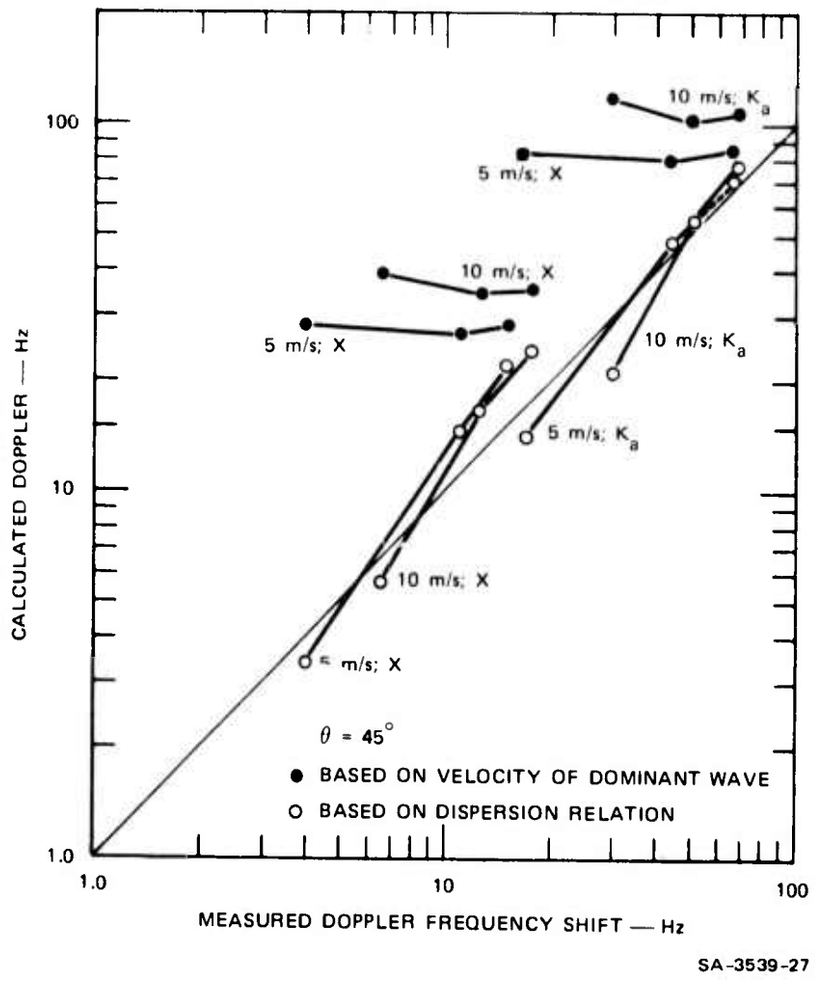

FIGURE 22 COMPARISON OF MEASURED AND CALCULATED DOPPLER SHIFT BASED ON SURFACE VALUE OF CURRENTS

IV PREDICTED PERTURBATION OF CROSS SECTION

Physical Dynamics, Inc. (PDI) has supplied SRI with predictions of the perturbation to the wavenumber spectrum caused by a "favorable" (flow-with-wind) or "adverse" (flow-against-wind) current.[1,2,6] Basically, these calculations predict that the greatest effect occurs at wavenumbers where the spectrum is developing. The perturbation at low wavenumbers is referred to as a "current gradient effect," and the perturbation at high wavenumbers is referred to as the "cutoff perturbation." Thus, the wavenumbers affected by an induced current can be expected to depend on the fetch and windspeed.

The PDI calculation show the perturbed spectrum Y normalized by the corresponding spectrum without flow, Y_o. This ratio of spectra should be directly related to similar ratios of cross section. Figures 23 to 26 show the calculated perturbation to the spectra along the length of the tank. The x coordinate in these figures is measured in feet relative to the leading edge of the false bottom. The wavenumbers for each of these four figures correspond roughly to those for which X-band and K_a-band data were given in Figures 6 through 9. Figures 23 and 24, which are for approximately the same wavenumber (corresponding to X-band scatter for $\theta = 45°$), show the effects of currents for wind speeds of 5-m/s and 10-m/s. As the wind increases, particular wavenumbers are perturbed at shorter fetches, because waves at any particular wavenumber are developing at shorter fetches. Similar behavior is also seen in Figures 25 and 26 (Figures 25 and 26 are also for approximately the same wavenumber). In Figure 26, the perturbation has apparently moved to a shorter fetch which is not near the false bottom, and consequently does not see the induced current effect.

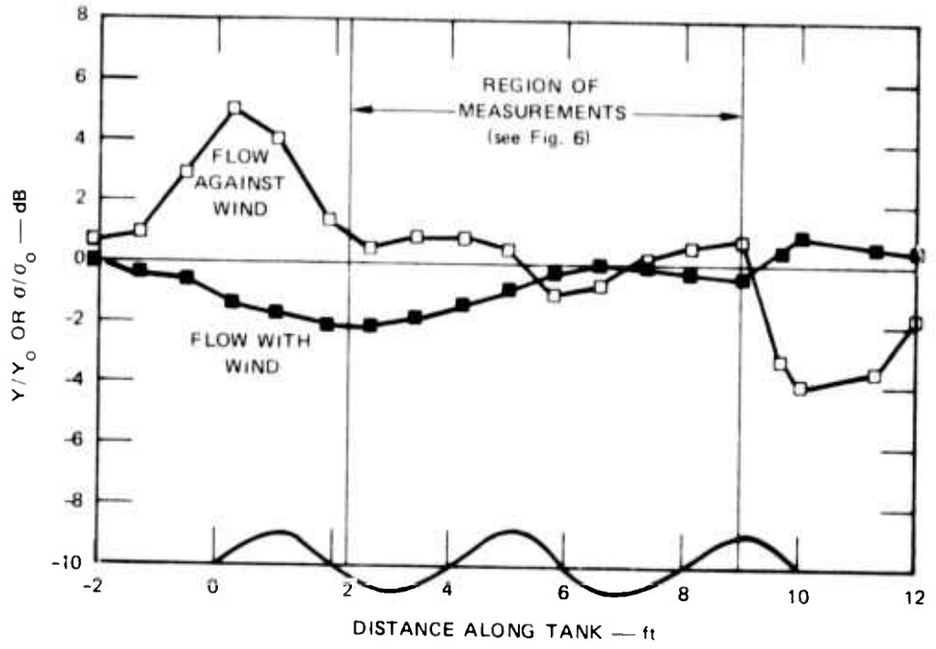

FIGURE 23 CALCULATED SPECTRAL PERTURBATION vs FETCH FOR k_w = 3.07 cm^{-1} AND U_N = 5 m/s

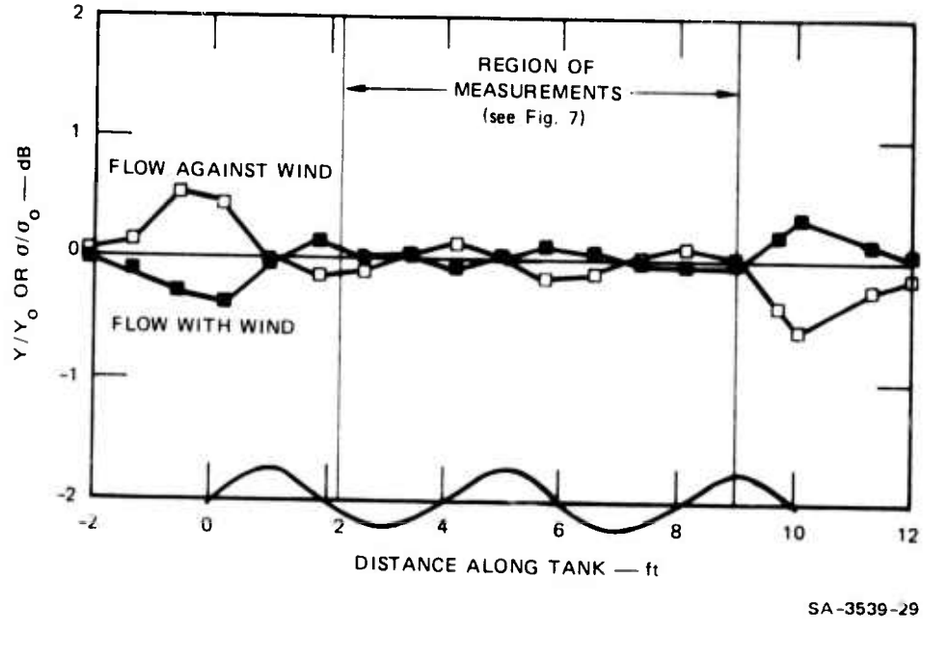

FIGURE 24 CALCULATED SPECTRAL PERTURBATION vs FETCH FOR k_w = 3.27 cm^{-1} AND U_N = 10 m/s

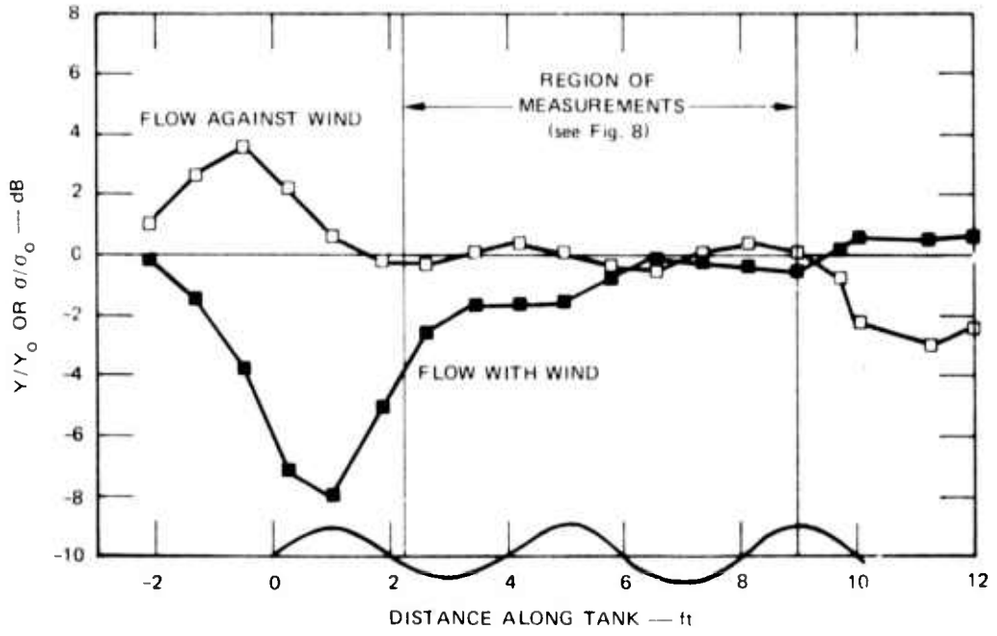

FIGURE 25 CALCULATED SPECTRAL PERTURBATION vs FETCH FOR k_w = 8.09 cm^{-1} AND U_N = 5 m/s

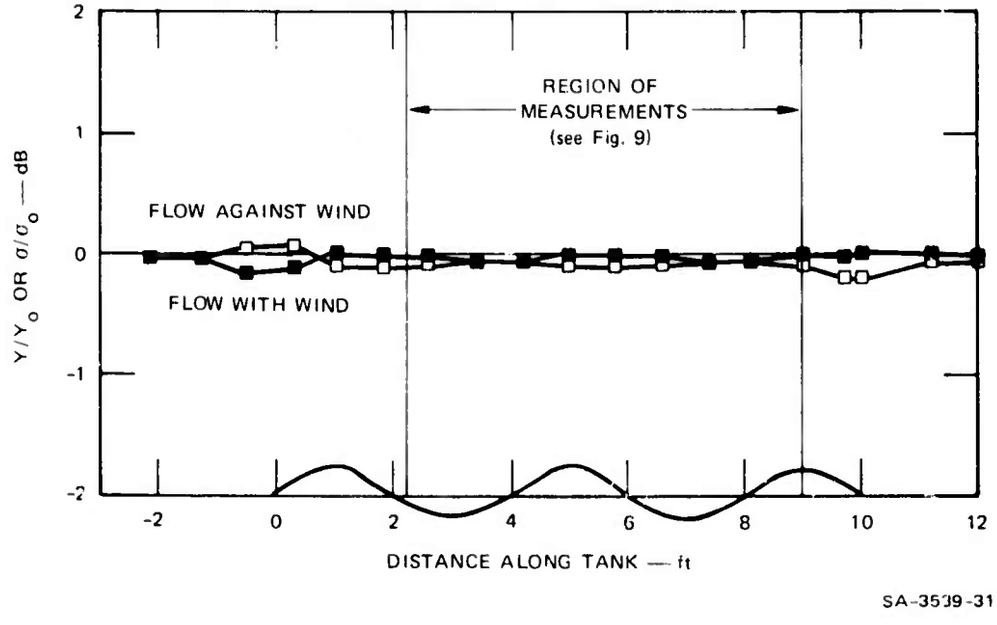

FIGURE 26 CALCULATED SPECTRAL PERTURBATION vs FETCH FOR k_w = 8.62 cm^{-1} AND U_N = 10 m/s

For a 5 m/s wind, the X-band flow-against-wind cross section, shown in Figure 23, is predicted to be about 1 dB greater than the no-flow cross section at the upward end of the measurement region, fall to about 0 dB at the 6-foot position, and rise to about +1 dB again at the downwind end of the false bottom. That is, virtually no change is predicted across the measurement region; the corresponding measured data in Figure 6 does show such a tendency. For the same wind speed, the X-band flow-with-wind cross section is predicted to be about 2 dB below the no-flow cross section at the upwind end of the measurement region, and to increase to about 0 dB at the downwind end of the measurement region. Similar behavior is seen in the measured data of Figure 6.

For a 10 m/s wind, the X-band flow-with-wind and flow-against-wind cross sections are both predicted to be approximately equal to the no-flow cross section along the length of the measurement region, as seen in Figure 24. This behavior is seen in the flow-against-wind data of Figure 7, although the flow-with-wind data shows a slight tendency to decrease toward the downwind end of the measurement region (it is about 1.5 dB below the no-flow data at the downwind end of the region, in Figure 7).

The K_a-band 5-m/s flow-with-wind cross section is predicted to increase from -4 dB at the upwind end of the measurement region to about 0 dB at the downwind end, as shown in Figure 25. Similar behavior is seen in the measured data of Figure 8. The corresponding flow-against-wind cross section is predicted to be approximately equal to the no-flow cross section across the measurement region; the measured data of Figure 8 shows a tendency to resemble the behavior of the flow-with-wind data rather than the no-flow data. The discrepancy, although not dramatic, is most noticeable at the upwind end, where it is approximately 5 dB.

The K_a-band 10-m/s cross sections are predicted to be approximately equal to the no-flow cross section, across the measurement region, as seen in Figure 26. The measured data of Figure 9 shows a similar lack of variation across the measurement region, although the flow-against-wind data is seen to be about 3 dB higher than predicted and the flow-with-wind data is 1.5 dB lower than predicted at the downwind end.

Figure 27 shows the calculated and measured perturbation at two positions on the false bottom, plotted against wavenumber. The measurements, made at two angles of incidence and at two frequencies, enabled a check to be made of this prediction at four wavenumbers. It is clear that the predicted 15-dB enhancement in cross section at the lowest

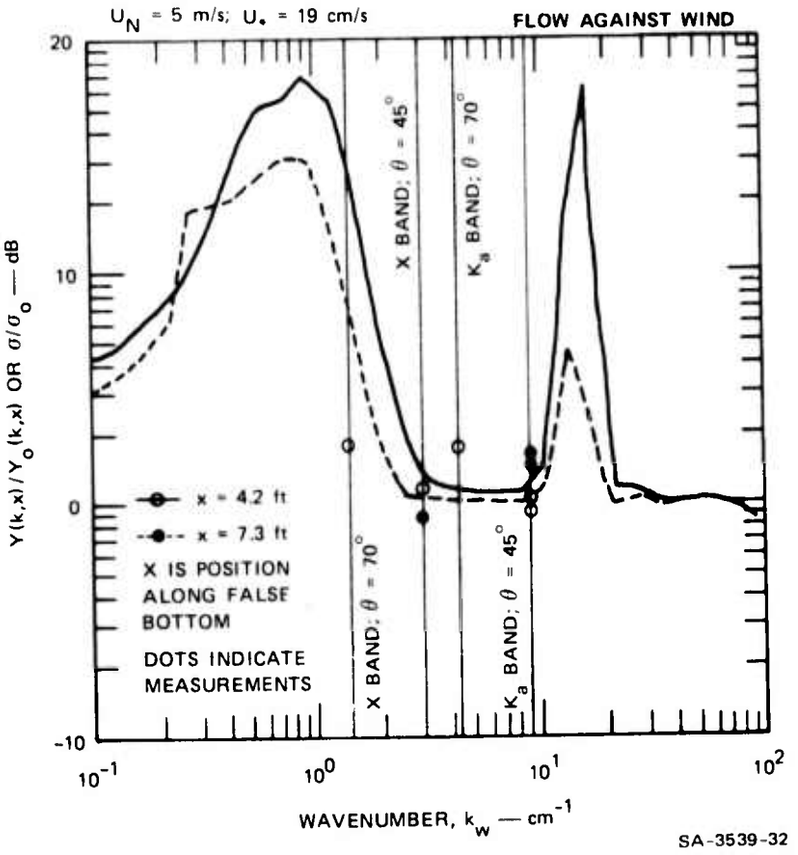

FIGURE 27 COMPARISON OF PREDICTED SPECTRAL PERTURBATIONS WITH MEASURED CROSS-SECTION PERTURBATIONS

wavenumber (X-band, $\theta = 70°$, $k_w = 1.43\ cm^{-1}$), at a position 4.2 ft from the leading edge of the false bottom was not observed. Only a 2-dB enhancement was observed. The predicted and measured perturbations in cross section at the other three wavenumbers are more nearly in agreement, as seen in Figure 27, than at the lowest wavenumber. (The calculations in Figure 27 were for an adverse flow; no similar calculation with wavenumber as a parameter was made for a favorable flow.)

V CONCLUSIONS

Measurements have been made to establish the effect of induced current on backscatter from wind-driven waves. A varity of microwave measurements were made; diagnostic wave-height measurements were made using resistance-wire wavestaffs. The effect of the induced current is readily apparent on wavestaff-measured spectra and in microwave Doppler-shift data. Perturbations in the radar backscatter cross-sections due to a 40-cm/s change in the induced current were also observed. However, perturbations in cross section due to induced current modulation caused by the corrugations in the false bottom were not observed. Backscatter cross section perturbations were compared to a theoretical prediction by Physical Dynamics, Inc. (PDI).

In general, the measured variation of cross section across the measurement region was in approximate agreement with the PDI prediction. The most serious discrepancy between the measured and predicted cross section perturbations occurred at a position 4.2 ft downwind from the leading edge of the false bottom, for a wavenumber k_w at 1.43 cm^{-1}. In this case, the measured perturbation (2 dB) was much lower than the predicted perturbation (15 dB). Generally, large perturbations were not observed at the fetches where measurements were made, whether predicted or not.

On the average, for 10-m/s wind at X-band, the cross-section data for flow against the wind was about 2-dB higher than for flow with the wind. That is, a total change of 2-dB was observed for a change in induced current of about 40-cm/s. For the K_a-band data, the total change was about 4-dB for a 40-cm/s current change. The corresponding changes in cross section for 5 m/s wind were similar at X-band and negligible at

K_a-band. In view of the observed change in cross section for a 40-cm/s change in current, it is not surprising that no perturbation was detected that coincided with the corrugations of the false bottom, which produced current "modulation" of about 5-cm/s.

One cross-correlation measurement between a pair of wavestaffs indicated that the wave components measured with the wavestaffs were being convected at the velocity of the dominant wave. This agrees with earlier measurements and implies that the wavestaffs are predominantly measuring parasitic waves over most of the low-frequency portions of the spectra. The microwave Doppler-shift data indicate that the radars are scattering from free waves, traveling at their own dispersion velocity rather than at the velocity of the dominant waves. In order to establish the relative importance of parasitic and free wave components responsible for backscatter, wavestaff measurements with more dynamic range would be required. From the wavestaff and microwave measurements, it is apparent that any theory which relates cross section to the wave components must distinguish between scattering from free and parasitic waves.

VI RECOMMENDATIONS

The measurements and theoretical calculations discussed in this report are in disagreement at low wavenumbers (see Figure 27). The reason for the disagreement is not clear. More detailed measurements at other locations in the tank could determine if and where the significant perturbations occurred, and how large they were. (Note that significant perturbations were in many cases predicted to occur upwind of the measurement region, where the spectra were developing.) The idea that the perturbation occurred at wavenumbers where the spectra were developing could be checked by careful wavestaff measurements of the wavenumber spectra. The 4-ft wavelength corrugations on the false bottom are now felt to produce a perturbation that is not very significant. PDI has suggested an experiment in which the false bottom is contoured to produce currents that simulate the orbital velocity of swell, with as long a wavelength as practicable. Such induced currents should produce an interaction with meter waves. Only an insignificant term, proportional to $\sqrt{K/k}$, that represents the effect of gravity would be ignored in the simulation. (The wavenumbers of the swell and meter waves are K and k, respectively.) The interaction with short waves that are responsible for microwave scatter is predicted to vary linearly with the meter-wave perturbation, and the measurements would give the value of the coupling coefficient describing this interaction. It is felt that such an experiment would be beneficial because the interaction of swell and meter waves is felt to be well understood, but the coupling to the capillaries is more difficult to establish.

Finally, while measurements at large angles of incidence are useful for checking theoretical predictions, experimental backscatter data

obtained at small angles of incidence would be valuable. Such measurements could be made in the wind-wave tank. Resolution of about 8 ft can be obtained for angles of incidence of about 5 degrees. As an additional benefit, induced currents could be pumped over a section of false bottom that was as large as the scattering area, and empirical data could be obtained that would specify the effects of currents at or near grazing incidence.

Appendix

WAVE DISPERSION

Appendix

WAVE DISPERSION

Figure A-1 shows the frequency dependence of velocity U(f) and wavenumber $k_w(f)$ when surface tension is important, based on relations in Kinsman:[7]

$$U^2(f) = g/k_w + Tk_w/\rho \qquad \text{(A-1)}$$

where g is the acceleration due to gravity; T is the surface tension, taken as 74 dynes/cm; and ρ is density. It is convenient to calculate

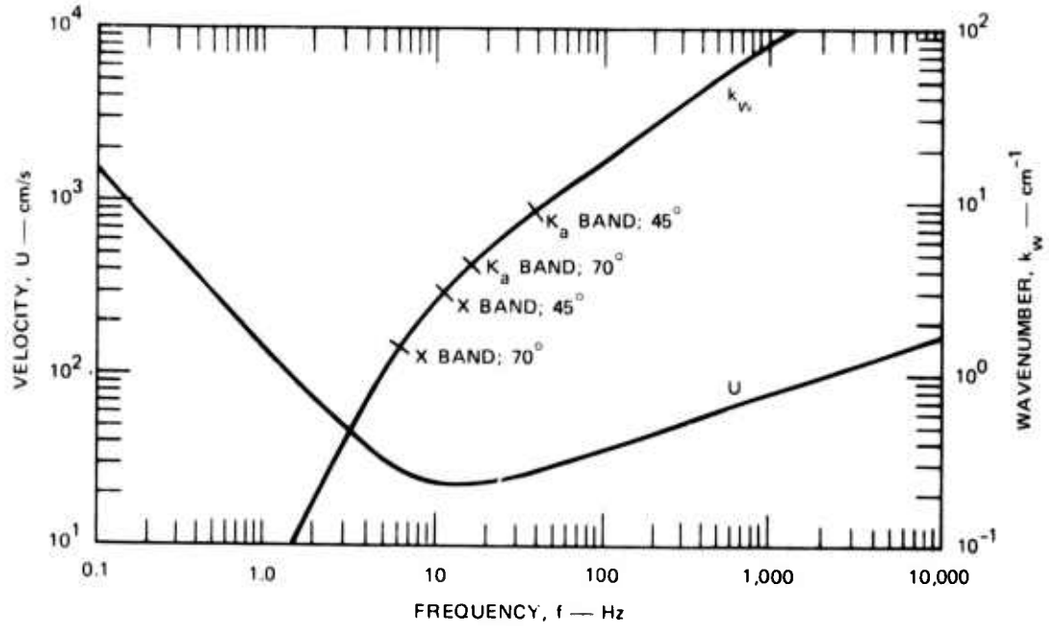

FIGURE A-1 VELOCITY AND WAVENUMBER DEPENDENCE ON FREQUENCY

U and f from the above formula, using k_w as the independent variable, and the following relation:

$$f = U/\lambda_w$$

$$= Uk_w/2\pi \quad . \tag{A-2}$$

ACKNOWLEDGMENTS

We would like to thank R. L. Warner for making the experimental measurements, and J. A. Martin for helping to process and reduce the data. We also thank W. E. Scharfman and T. Morita, of SRI, and J. A. Thomson and B. J. West, of PDI for many helpful discussions.

REFERENCES

1. J. A. Thomson and B. J. West, "Interaction of Non-Saturated Surface Gravity Waves with Internal Waves," PD-72-023, Technical Report, Contract F30602-72-C-0494, Physical Dynamics, Inc., Berkeley, Calif. (October 1972).

2. J. A. Thomson and B. J. West, "Review of Ocean Wave-Surface Current Interaction: Theory and Experiment," PD-74-056, Contract F30602-72-C-0494, Report, Chapter 4, Physical Dynamics, Inc., Berkeley, Calif. (1974).

3. H. Guthart, W. C. Taylor, K. A. Graf, and D. G. Douglas, "Correlation Techniques and Measurements of Wave Height Statistics," Final Report, Contract NAS1-10681, SRI Project 1183, Stanford Research Institute, Menlo Park, Calif. (May 1972).

4. O. M. Phillips, The Dynamics of the Upper Ocean (Cambridge University Press, Cambridge, Mass., 1966).

5. J. W. Wright and W. C. Keller, "Doppler Spectra in Microwave Scattering from Wind Waves," Phys. Fluids, Vol. 14, No. 3, pp. 466-475 (March 1971).

6. J. A. Thomson and B. J. West, private communication.

7. B. Kinsman, Wind Waves (Prentice-Hall, Englewood Cliffs, New Jersey, 1965).